Letter

Electron correlations in the kagome flat band metal $CsCr_3Sb_5$

Fang Xie,[1,2] Yuan Fang,[1] Ying Li,[3] Yuefei Huang,[4] Lei Chen,[1] Chandan Setty,[1,5,6] Shouvik Sur,[1] Boris Yakobson,[4] Roser Valentí,[7] and Qimiao Si[1]

[1]*Department of Physics & Astronomy, Rice Center for Quantum Materials, Rice University, Houston, Texas 77005, USA*
[2]*Rice Academy of Fellows, Rice University, Houston, Texas 77005, USA*
[3]*MOE Key Laboratory for Nonequilibrium Synthesis and Modulation of Condensed Matter, School of Physics, Xi'an Jiaotong University, Xi'an 710049, China*
[4]*Department of Materials Science and NanoEngineering, Rice University, Houston, Texas 77005, USA*
[5]*Department of Physics and Astronomy, Iowa State University, Ames, Iowa 50011, USA*
[6]*Ames National Laboratory, U.S. Department of Energy, Ames, Iowa 50011, USA*
[7]*Institut für Theoretische Physik, Goethe-Universität Frankfurt, Max-von-Laue-Strasse 1, 60438 Frankfurt am Main, Germany*

(Received 23 September 2024; accepted 22 April 2025; published 10 June 2025)

Kagome metals offer a unique platform for investigating robust electron-correlation effects because of their lattice geometry, flat bands, and multiorbital nature. In the cases with active flat bands, recent theoretical studies have pointed to a rich phase diagram that contains not only electronic orders but also quantum criticality. Very recently, $CsCr_3Sb_5$ has emerged as a strong candidate for exploring such new physics. Here, using effective tight-binding models obtained from *ab initio* calculations, we study the effects of electronic correlations and symmetries on the electronic structure of $CsCr_3Sb_5$. The effective tight-binding model and Fermi surface comprise multiple Cr-*d* orbitals and Sb-*p* orbitals. The introduction of Hubbard-Kanamori interactions leads to orbital-selective band renormalization dominated by the d_{xz} band, concurrently producing emergent flat bands very close to the Fermi level. Our analysis sets the stage for further investigations into the electronic properties of $CsCr_3Sb_5$, including electronic orders, quantum criticality, and unconventional superconductivity, which promise to shed much new light into the electronic materials with frustrated lattices and bring about new connections with the correlation physics of a variety of strongly correlated systems.

DOI: 10.1103/PhysRevResearch.7.L022061

Introduction. Materials with flat bands from frustrated lattices provide a distinctive venue to explore the intersection of lattice geometry, strong correlation effects, and multiorbital physics [1–10]. Experiments in such materials have found evidence for non-Fermi liquid behavior [11–13]. Theoretically, the coupling between the flat and wide bands has been shown to yield a formation of local moment from compact molecular orbitals [14–16] and the development of electronic orders, with the quantum critical regime displaying strange metal behavior [14,16]. The recent discovery of $CsCr_3Sb_5$ [17], a Cr-based kagome material, has opened an exciting avenue [18] for exploring this rich physics while adding a distinct new member to the kagome material family [19]. With its unique phenomenology and multiorbital nature, this system offers a rare opportunity to examine the robust effects of electron correlation in a flat-band platform.

$CsCr_3Sb_5$ is isostructural to the more familiar vanadium-based kagome material family AV_3Sb_5 ($A = \mathrm{Cs, K, Rb}$) [20–23]. It is a bad metal at ambient pressure supporting the existence of strong correlation effects. Anomalies in transport and thermodynamic properties suggest multiple ordering transitions as a function of temperature and pressure [17]. While the nature of the order is presently unclear, it has a single ordering wave-vector modulation, involving a hexagonal to monoclinic distortion [17]. This is different from the behavior observed in the vanadium family [4,24–29].

Equally important, high temperature susceptibility data in $CsCr_3Sb_5$ shows a Curie-Weiss behavior indicating the formation of local moments. High pressure suppresses the density-wave ordering, leading to domelike unconventional superconductivity separated by a putative quantum critical points; in contrast, the AV_3Sb_5 family exhibits ambient pressure superconductivity, which persists under pressure [23]. In addition, resistivity data indicates strong deviations from Fermi-liquid behavior further supporting the role of strong correlations and quantum criticality [17].

Here, we study the low-energy correlated electronic properties of $CsCr_3Sb_5$, including its flat band behavior near the Fermi energy and Fermi surface characteristics that shape the physical properties of this material; importantly, we rest our understanding of the low-energy electronic states on a comprehensive symmetry analysis. We clarify the role of strong correlation effects on the electronic structure by investigating the suppression of the orbital-dependent quasiparticle weights using the slave-spin approach. We begin by identifying the site-symmetry groups and representations of Wyckoff

Published by the American Physical Society under the terms of the Creative Commons Attribution 4.0 International license. Further distribution of this work must maintain attribution to the author(s) and the published article's title, journal citation, and DOI.

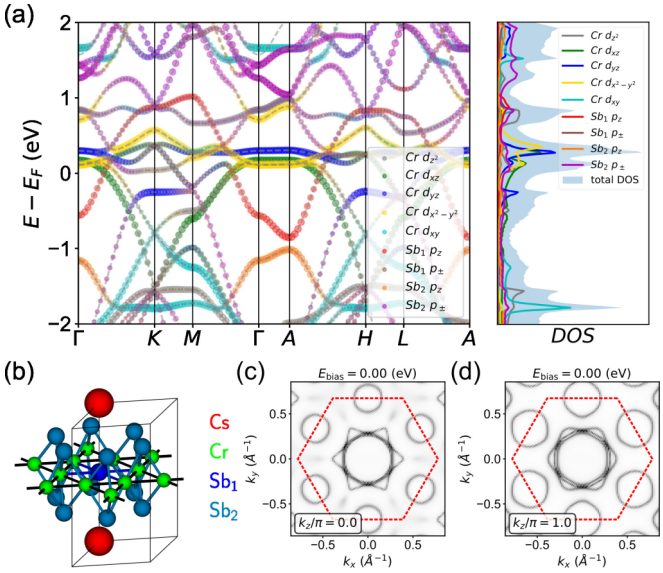


FIG. 1. (a) Band structure and density of states of $CsCr_3Sb_5$ compound obtained from density functional theory using VASP and GGA. The color codes represent the orbital content of the corresponding Bloch states. (b) The lattice structure of $CsCr_3Sb_5$. Black box stands for the unit cell. (c), (d) Momentum-resolved spectral function at $k_z = 0$ and $k_z = \pi$ planes at the Fermi energy obtained from the *ab initio* band structure. The red dashed line stands for the first Brillouin zone. Electron pockets near the M points, electron, and hole pockets around the Γ point can be seen in this spectral function. Spin-orbital-coupling (SOC) is not considered.

positions of the space group $P6/mmm$, which correspond to the lattice sites of Cr and Sb atoms. We then analyze the band structure obtained from *ab initio* calculations, which identify the orbitals from the Cr and Sb atoms that are relevant to the low-energy physics and lead to a tight-binding model. We find that the Hubbard-Kanamori-type interactions [30,31] induce strong orbital-selective renormalization effects in the Cr-d orbitals, especially the d_{xz} orbital. Additionally, our analysis reveals that strong correlations lead to a noticeably larger spectral weight near the Fermi level, in contrast to the prediction of *ab initio* studies. In other words, the correlations generate an emergent flat band very close to the Fermi energy. Our investigation sets the stage for further research into the nature of the unusual electronic order, quantum criticality, and superconductivity of this promising new material.

Symmetry and effective model. The $CsCr_3Sb_5$ compound has nine atoms per unit cell. As shown in Fig. 1(b), there are three Cr atoms forming a kagome lattice. Among the five Sb atoms, one of them is at the center of the hexagon plaquette of the chromium kagome lattice within the Cr plane denoted as Sb_1, while the other four are at out-of-plane positions denoted as Sb_2, forming two sets of hexagonal lattices. Besides, the Cs atom is positioned atop of Sb_1 in a separate plane.

The active orbitals near the Fermi level are the Cr-3d orbitals, and the Sb-5p orbitals. Indeed, these orbitals are all responsible for the low energy physics near the Fermi level, as suggested by *ab initio* studies [17,32]. In Fig. 1(a) we provide the band dispersion, whose color codes stand for the weights of different orbital content, and the corresponding density of states (DOS) obtained from density functional theory using VASP [33,34] and GGA [35]. The total density of states approaches its peak at around ∼0.3 eV above the Fermi level, which is mostly formed by the Cr-d_{xz} and d_{yz} orbitals. The d_{z^2} and $d_{x^2-y^2}$ orbitals are also responsible for states close to E_F. Except for these Cr orbitals, we also found that the Sb_1-p_z orbital provides an electron pocket near the Γ point, which is highlighted by the red markers in Fig. 1(a). The Sb_2-$p_\pm$ and p_z orbitals also strongly hybridize with the Cr-d orbitals, which lead to non-negligible contributions to the band structure near E_F.

TABLE I. Irreducible representations of d orbitals in the point group mmm (D_{2h}) of the $3f$ Wyckoff position of space group 191. Since all d orbitals have inversion eigenvalue +1, the three twofold rotations distinguish their irreps.

E	C_{2x}	C_{2y}	C_{2z}	irrep	orbital
+1	+1	+1	+1	A_g	$d_{z^2}, d_{x^2-y^2}$
+1	−1	−1	+1	B_{1g}	d_{xy}
+1	−1	+1	−1	B_{2g}	d_{xz}
+1	+1	−1	−1	B_{3g}	d_{yz}

We show the momentum resolved spectral function at the Fermi level with different k_z values obtained from the *ab initio* band structure in Figs. 1(c) and 1(d). Three electron pockets near the M points, which are mostly formed by Cr-d_{xz} and d_{yz} orbitals, are easily visible. Furthermore, we observe near the Γ point one electron pocket formed by the Sb-p_z orbital, and hole pockets formed by Cr-d_{xz}, d_{z^2} and $d_{x^2-y^2}$ orbitals. The similarity in the Fermi pockets at $k_z = 0$ and $k_z = \pi$ planes also shows the two-dimensional nature of this material.

This *ab initio* analysis delineates the degrees of freedom that are important for the electronic structure of $CsCr_3Sb_5$. Since there are many orbitals contributing to the low energy physics, it is a challenging task to build a reliable model to capture the relevant physics while not being unnecessarily complicated.

To make progress, we first analyze the crystalline symmetry. The space group of $CsCr_3Sb_5$ is $P6/mmm$ (no. 191). The Wyckoff positions, site-symmetry groups, and irreducible representations (irrep) of these active atomic orbitals are discussed as follows [36,37].

(1) The Cr-d orbitals are at the $3f$ Wyckoff position (kagome sites). Each of the orbitals forms a one-dimensional irrep of the site-symmetry group mmm (D_{2h}). Since all d orbitals have inversion eigenvalue +1, their representations are uniquely determined by the quotient group 222 (D_2). In Table I, we provide the character table and the representations of the d-orbitals of this point group. The local coordinate basis for each kagome site is selected in accordance with the principle axes of the site symmetry group, as labeled in Fig. 2(a).

(2) The Sb_1-p_z orbital is at the $1b$ Wyckoff position (triangular sites) which forms the irrep A_{2u} of the site-symmetry group $6/mmm$ (D_{6h}). The Sb_1-$p_\pm$ orbitals form the irrep E_{1u} of the site-symmetry group $6/mmm$.

(3) The Sb_2-p_z and $p_\pm$ orbitals are at the $4h$ Wyckoff position which form the one-dimensional irrep A_1 and

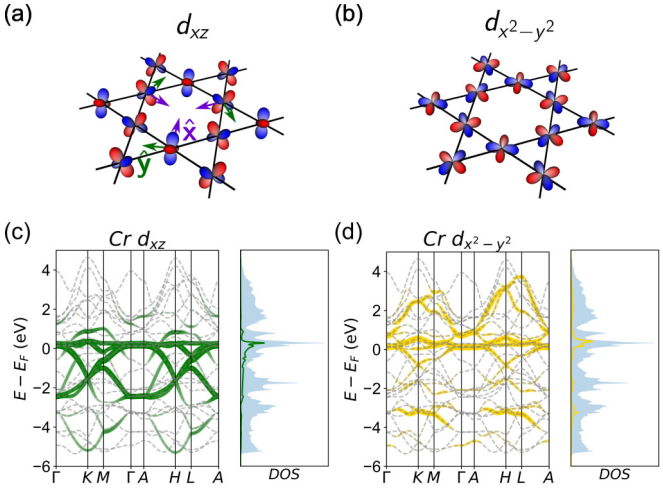


FIG. 2. (a) The shape of the d_{xz} orbitals on the chromium atoms. The basis vectors $\hat{\mathbf{x}}, \hat{\mathbf{y}}$ of local coordinate frames on each kagome site are represented by the purple and green arrows, respectively. Note that the orientation of the principle axes on different kagome sites are chosen differently. (b) The shape of the $d_{x^2-y^2}$ orbitals on the chromium atoms. (c) Band structure and the density of states (DOS) projected onto the d_{xz} orbitals. (d) Band structure and the DOS projected onto the $d_{x^2-y^2}$ orbitals. In the DOS plots, the light blue shadows stand for the total DOS.

two-dimensional irrep E of the site-symmetry group $3m$ (C_{3v}), respectively.

(4) One empty Cs band is around 2 eV above the Fermi level, which also hybridizes with multiple Sb-p orbitals. The Cs-s orbital is at the $1a$ Wyckoff position which forms the irrep A_{1g} of the site-symmetry group $6/mmm$ (D_{6h}).

By projecting the *ab initio* Bloch states onto these atomic orbitals, one can construct an effective tight-binding model with $31 = 1 \times 1(\text{Cs-}s) + 3 \times 5(\text{Cr-}d) + 5 \times 3(\text{Sb-}p)$ orbitals and $34 = 1 \times 1(\text{Cs-}6s^1) + 3 \times 6(\text{Cr-}3d^5 4s^1) + 5 \times 3(\text{Sb-}5p^3)$ valence electrons per unit cell using WANNIER90 [38]. Note that all of the five d orbitals on each of the Cr atoms are taken into account in this tight-binding model. As such, this tight-binding model can faithfully describe the energy bands in the interval $-6\,\text{eV} < E - E_F < 5\,\text{eV}$.

In Figs. 2(c) and 2(d), we provide the "fat bands" projected onto the d_{xz} and $d_{x^2-y^2}$ orbitals on the 31-band tight-binding model, with their corresponding DOS plots. The "fat bands" plots of the other three types of d orbitals are shown in Fig. S1 of the Supplemental Material (SM) [39]. Due to the strong hybridization between the Cr-d orbitals and the Sb-p orbitals, states that are a few electron volts away from the Fermi level still possess non-negligible DOS from these Cr-d orbitals. Among the five d orbitals, we found that the DOS of the d_{xz} orbital has the smallest spread, while those of the d_{yz} and $d_{x^2-y^2}$ orbitals have larger spreads than for the other orbitals. These results indicate that the d_{xz} orbital has a weaker hybridization strength with the other orbitals, suggesting that it will have the strongest renormalization when the interaction effects are considered. In addition, it is also noticeable that all of these five Cr-d orbitals are relevant to the electronic states near the Fermi level. Hence, any truncated effective models with a subset of these orbitals on Cr atoms are unlikely to be faithful.

Interaction effects. As addressed in the previous section, an effective model with truncated Cr-d orbitals is not suitable for accurately describing correlation effects in low-energy physics. Therefore, a proper treatment of interaction terms should include all these Cr-d orbitals, with the Cs-s and Sb-p orbitals as the "conduction bath" states. We choose a Hubbard-Kanamori-type Hamiltonian to describe the correlation effects [30,31], which contains the on-site repulsive interaction and Ising-type ferromagnetic Hund's coupling terms for all five Cr-d orbitals:

$$H_I = U \sum_{j\alpha} \tilde{n}_{j\alpha\uparrow}\tilde{n}_{j\alpha\downarrow} + U' \sum_{j,\alpha\neq\beta} \tilde{n}_{j\alpha\uparrow}\tilde{n}_{j\beta\downarrow} + (U' - J_H) \sum_{j,\alpha<\beta,\sigma} \tilde{n}_{j\alpha\sigma}\tilde{n}_{j\beta\sigma}. \quad (1)$$

Here j stands for the kagome lattice sites, $\alpha, \beta = 1, 2, ..., 5$ mark the Cr-d orbital indices, and $\sigma = \uparrow, \downarrow$ describes the electron spin. The operator $\tilde{n}_{j,\alpha,\sigma} = c^\dagger_{j,\alpha,\sigma} c_{j,\alpha,\sigma} - \frac{1}{2}$ represents the (relative) electron density on orbital α with spin σ at site j. The bare on-site Coulomb interaction on the Cr-d orbitals is estimated to be around $U_{\text{bare}} \approx 12 \sim 15\,\text{eV}$. However, screening effects and the type of chemical environment of Cr reduce the effective interaction strength to values around $3 \sim 6\,\text{eV}$ [40,41].

The interacting Hamiltonian in the correlated metallic phases can be studied by the $U(1)$ slave-spin approach [39,42,43]. In this framework, the quasiparticle weights and the on-site potential renormalization for each orbital can be solved self-consistently [44]. The meaning of these renormalization factors is two-fold: (i) the quasiparticle weights which are smaller than unity indicate the suppression of the kinetic energies and the effective hybridization strength in the coherent Fermi liquid excitations; (ii) the on-site potential renormalizations may lead to charge transfer among different orbitals, while ensuring that the total filling factor remains unchanged when the interaction strength is varied. With both renormalization factors considered, the dispersion of the coherent Fermi liquid excitations can be solved. In addition, the shape and the orbital contents of the Fermi surface may vary when the interactions are taken into consideration, due to orbital-selective nature of the correlation effects.

Here we solve the interacting Hamiltonian with interaction strength $0 \leqslant U \leqslant 6\,\text{eV}$ and Hund's coupling $J_H/U = 0.2$ at a fixed filling factor. Our results indicate that (i) the orbital-selective correlation effects exist, and the d_{xz} orbital experiences the strongest renormalization; (ii) the narrow bands are pinned near the Fermi energy, leading to a considerable reduction in the energetic separation between the Fermi level and the peak of the DOS from the *ab initio* value of 0.3 eV. Below, we further elaborate on our discussion regarding these points.

Orbital-selective Mott correlation. The quasiparticle weights of all the five d orbitals as functions of the interaction strength U are provided in Fig. (3). Significantly, the quasiparticle weights are strongly renormalized when the interaction strength U is increased above 4 eV. Moreover, the renormalization effects on distinct d orbitals are different from each

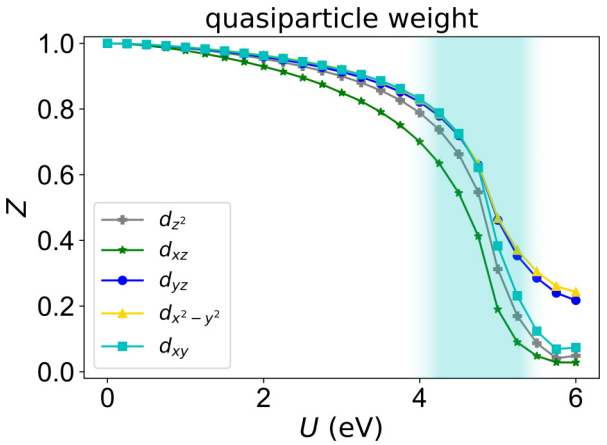


FIG. 3. The quasiparticle weights and electron occupation numbers (per spin) of the five Cr-d orbitals, computed as functions of the interaction strength $0 \leqslant U \leqslant 6\,\text{eV}$. The d_{xz} orbital shows the strongest renormalization effect with large interaction strength $U \gtrsim 4\,\text{eV}$. In the region highlighted by the cyan shadow, the d orbitals' quasiparticle weights drop significantly. The Hund's coupling strength is chosen to be $J_H = 0.2U$ in this calculation.

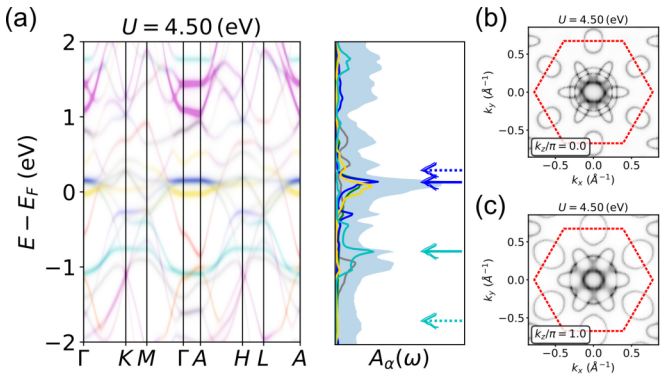


FIG. 4. (a) Momentum resolved spectral functions of the coherent excitations, $A_\alpha^{\text{coh}}(\mathbf{k}, \omega)$, and the density of states obtained from the slave-spin approach with the interaction strength $U = 4.5\,\text{eV}$. The color codes are the same as labeled in Fig. 1. The dashed arrows stand for the peaks of DOS with $U = 0$, while the solid arrows mark the peaks of DOS with $U = 4.5\,\text{eV}$. The color codes of the orbital contents are the same as in Fig. 1(a). (b), (c) Fermi surface plots in the $k_z = 0$ and $k_z = \pi$ planes.

other. In brief, the d orbitals which have weaker hybridization or smaller hoppings to other orbitals are more likely to be renormalized. Indeed, as shown in Fig. 3, the quasiparticle weight of the d_{xz} orbital drops the most rapidly with increasing interaction U. In contrast, the Z_α values of the $d_{x^2-y^2}$ and d_{yz} orbitals are also noticeably larger than other d orbitals, especially when $U \gtrsim 5\,\text{eV}$. Additionally, we observe that if U is increased to $\sim$6 eV, which is still within a reasonable range [40,41], the three orbitals (d_{xz}, d_{z^2}, and d_{xy}) are strongly renormalized with quasiparticle weights $Z \lesssim 0.1$. This indicates that the system is approaching an orbital-selective Mott transition, during which the quasiparticle weights of one or more orbitals decay to zero.

Emergent flat band near Fermi level. Correlation effects on the quasiparticle weights and on-site potentials lead to the suppression of the kinetic energy and hybridization effects in the coherent Fermi liquid spectrum. In Fig. 4(a), the orbital-resolved coherent fermion excitation spectrum $A_\alpha^{\text{coh}}(\mathbf{k}, \omega)$ and its corresponding DOS with interaction strength $U = 4.5\,\text{eV}$ are provided. The band structure is drastically changed compared to its noninteracting counterpart [Fig. 1(a)]. The dashed arrows in Fig. 4(a) label the position of two DOS peaks in the *ab initio* band structure, while the solid arrows are the corresponding peaks in the correlated DOS. The peak above E_F labeled by the blue arrow, which is mostly formed by d_{xz}, d_{yz}, and $d_{x^2-y^2}$ orbitals, now appears considerably closer to the Fermi energy. At the same time, the occupied "flat band" of the d_{xy} orbital, which is highlighted by the cyan arrows, is strongly pushed upward. Although the emergent "flat bands" of the coherent excitations appear near E_F, the reduction of the quasiparticle weights also leads to weaker intensities in the momentum resolved spectral functions. We note that the correlated flat bands still capture the destructive interference of the kagome lattice, since they can be adiabatically connected to the destructive-interference-induced flat bands in the DFT bandstructure when the interaction U is gradually reduced; this point is further discussed in the SM [39].

The correlated Fermi surfaces are also shown in Figs. 4(b) and 4(c). Due to the orbital-selective renormalization effects, the size and shape of Fermi pockets with different orbital contents will be changed. For example, the electron pockets around the three M points become smaller than the ones in Fig. 1(c). The concentric Fermi pockets around the Γ point, which are predominantly formed by p_z, d_{xz}, and $d_{x^2-y^2}$ orbitals, also show varying sizes compared to their counterparts in the absence of interactions. Moreover, another shallow electron pocket emerges around the Γ point, which is mostly formed by the $d_{x^2-y^2}$ orbital. Additional discussion regarding the correlated Fermi surfaces with different interaction strengths U can be found in the SM [39].

Discussion. Given that $CsCr_3Sb_5$ is strongly correlated with active flat bands, and considering the extensive ongoing interest in its more weakly correlated V-based counterpart [23], we can expect this Cr-based kagome material to reveal much insight into the strong correlation physics of metallic systems with geometrically frustrated lattices beyond what one can from their V-based counterparts. Here we have analyzed its electronic states. Based on an effective model that faithfully describes the *ab initio* band structure, we are able to systematically study the correlation effects on the Cr-d orbitals. Our results demonstrate strong renormalization effects when the interaction strength is within a reasonable and realistic range. A recent study [45] using the DFT + DMFT approach reached compatible conclusions regarding the renormalization effects, though it did not address either the Fermi surface under correlation or systematic symmetry analysis.

Due to the inequivalence of the Cr-d orbitals as irreps of the point group D_{2h}, the correlation effects show a noticeable orbital-selective signature, with the d_{xz} orbital experiencing the largest renormalization. The strong correlation effect suggests that fluctuations in the spin and other collective channels will have considerable spectral weight, and this can be tested by neutron scattering or resonant inelastic x-ray spectroscopy.

Our study also provides predictions about the electronic structure of this material. We identify flat bands that lie in the immediate vicinity of the Fermi energy, in contrast to the noninteracting flat bands that appear about 0.3 eV away from the Fermi energy. Furthermore, we determine the shape and size of the Fermi pockets in the presence of interactions. These effects can be tested by measurements such as angle resolved photoemission spectroscopy and scanning tunneling microscopy. For example, the emergent flat band and related low-energy electronic properties that are predicted here have been observed by three independent experiments based on angle resolved photoemission spectroscopy [46–48].

Our construction and analysis of the electronic states based on crystalline symmetries set the stage for further in-depth study of the competing ground states and quantum criticality in this correlated material. The fact that d_{xz} and d_{yz} states dominate the low-energy regime suggests the construction of either corresponding quasimolecular orbitals [49,50] or the compact molecular orbitals [14–16] will have the advantage of incorporating the low-energy p and d states in a symmetry-compatible way and addressing the role of topology. Such real-space basis can also enable the treatment of competing effective interactions, responsible for both the development of electronic orders and the amplification of quantum fluctuations. In other kagome compounds, novel density wave phases that break time-reversal symmetry have been evidenced [6,9,51,52]; the extent to which such unusual electronic order develops in $CsCr_3Sb_5$, and how they entwine with the electronic topology [10,53] when considering the spin-orbit coupling [39], are additional fascinating questions for future studies.

Acknowledgments. We thank Pengcheng Dai, Ming Yi, Yucheng Guo, Zehao Wang, and Yiming Wang for useful discussions. Work at Rice has primarily been supported by the U.S. DOE, BES, under Award No. DE-SC0018197, and by the Robert A. Welch Foundation Grant No. C-1411. C.S. additionally acknowledges support from Iowa State University and Ames National Laboratory startup funds. The majority of the computational calculations have been performed on the Shared University Grid at Rice funded by NSF under Grant EIA-0216467, a partnership between Rice University, Sun Microsystems, and Sigma Solutions, Inc., the Big-Data Private-Cloud Research Cyberinfrastructure MRI-award funded by NSF under Grant No. CNS-1338099, and the Advanced Cyberinfrastructure Coordination Ecosystem: Services & Support (ACCESS) by the NSF under Grant No. DMR170109. Y.L. acknowledges funding by the National Natural Science Foundation of China (Grant No. 12004296). R.V. acknowledges funding by the Deutsche Forschungsgemeinschaft (DFG, German Research Foundation) through Project No. TRR 288 — 422213477 (Project A05). The work of Y.H. and B.Y. was supported by the U.S. Office of Naval Research grant N00014-22-1-2753.

[1] A. Mielke, Exact ground states for the Hubbard model on the kagome lattice, J. Phys. A: Math. Gen. **25**, 4335 (1992).

[2] Y.-P. Lin, C. Liu, and J. E. Moore, Complex magnetic and spatial symmetry breaking from correlations in kagome flat bands, Phys. Rev. B **110**, L041121 (2024).

[3] D. Călugăru, A. Chew, L. Elcoro, Y. Xu, N. Regnault, Z.-D. Song, and B. A. Bernevig, General construction and topological classification of crystalline flat bands, Nat. Phys. **18**, 185 (2022).

[4] Y.-X. Jiang, J.-X. Yin, M. M. Denner, N. Shumiya, B. R. Ortiz, G. Xu, Z. Guguchia, J. He, M. S. Hossain, X. Liu, J. Ruff, L. Kautzsch, S. S. Zhang, G. Chang, I. Belopolski, Q. Zhang, T. A. Cochran, D. Multer, M. Litskevich, Z.-J. Cheng, X. P. Yang, Z. Wang, R. Thomale, T. Neupert, S. D. Wilson, and M. Z. Hasan, Unconventional chiral charge order in kagome superconductor Kv_3Sb_5, Nat. Mater. **20**, 1353 (2021).

[5] M. Kang, S. Fang, L. Ye, H. C. Po, J. Denlinger, C. Jozwiak, A. Bostwick, E. Rotenberg, E. Kaxiras, J. G. Checkelsky, and R. Comin, Topological flat bands in frustrated kagome lattice cosn, Nat. Commun. **11**, 4004 (2020).

[6] C. Mielke III, D. Das, J.-X. Yin, H. Liu, R. Gupta, Y.-X. Jiang, M. Medarde, X. Wu, H. C. Lei, J. Chang, P. Dai, Q. Si, H. Miao, R. Thomale, T. Neupert, Y. Shi, R. Khasanov, M. Z. Hasan, H. Luetkens, and Z. Guguchia, Time-reversal symmetry-breaking charge order in a kagome superconductor, Nature (London) **602**, 245 (2022).

[7] S. Zhou and Z. Wang, Chern fermi pocket, topological pair density wave, and charge-4e and charge-6e superconductivity in kagomé superconductors, Nat. Commun. **13**, 7288 (2022).

[8] X. Teng, L. Chen, F. Ye, E. Rosenberg, Z. Liu, J.-X. Yin, Y.-X. Jiang, J. S. Oh, M. Z. Hasan, K. J. Neubauer, B. Gao, Y. Xie, M. Hashimoto, D. Lu, C. Jozwiak, A. Bostwick, E. Rotenberg, R. J. Birgeneau, J.-H. Chu, M. Yi, and P. Dai, Discovery of charge density wave in a kagome lattice antiferromagnet, Nature (London) **609**, 490 (2022).

[9] J.-X. Yin, Y.-X. Jiang, X. Teng, M. S. Hossain, S. Mardanya, T.-R. Chang, Z. Ye, G. Xu, M. M. Denner, T. Neupert, B. Lienhard, H.-B. Deng, C. Setty, Q. Si, G. Chang, Z. Guguchia, B. Gao, N. Shumiya, Q. Zhang, T. A. Cochran, D. Multer, M. Yi, P. Dai, and M. Z. Hasan, Discovery of charge order and corresponding edge state in kagome magnet FeGe, Phys. Rev. Lett. **129**, 166401 (2022).

[10] C. Setty, C. A. Lane, L. Chen, H. Hu, J.-X. Zhu, and Q. Si, Electron correlations and charge density wave in the topological kagome metal FeGe, arXiv:2203.01930.

[11] J. Huang, L. Chen, Y. Huang, C. Setty, B. Gao, Y. Shi, Z. Liu, Y. Zhang, T. Yilmaz, E. Vescovo, M. Hashimoto, D. Lu, B. I. Yakobson, P. Dai, J.-H. Chu, Q. Si, and M. Yi, Non-fermi liquid behaviour in a correlated flat-band pyrochlore lattice, Nat. Phys. **20**, 603 (2024).

[12] L. Ye, S. Fang, M. Kang, J. Kaufmann, Y. Lee, C. John, P. M. Neves, S. Y. F. Zhao, J. Denlinger, C. Jozwiak, A. Bostwick, E. Rotenberg, E. Kaxiras, D. C. Bell, O. Janson, R. Comin, and J. G. Checkelsky, Hopping frustration-induced flat band and strange metallicity in a kagome metal, Nat. Phys. **20**, 610 (2024).

[13] S. A. Ekahana, Y. Soh, A. Tamai, D. Gosálbez-Martínez, M. Yao, A. Hunter, W. Fan, Y. Wang, J. Li, A. Kleibert, C. A. F.

Vaz, J. Ma, H. Lee, Y. Xiong, O. V. Yazyev, F. Baumberger, M. Shi, and G. Aeppli, Anomalous electrons in a metallic kagome ferromagnet, Nature (London) **627**, 67 (2024).

[14] L. Chen, F. Xie, S. Sur, H. Hu, S. Paschen, J. Cano, and Q. Si, Metallic quantum criticality enabled by flat bands in a kagome lattice, arXiv:2307.09431.

[15] L. Chen, F. Xie, S. Sur, H. Hu, S. Paschen, J. Cano, and Q. Si, Emergent flat band and topological kondo semimetal driven by orbital-selective correlations, Nat. Commun. **15**, 5242 (2024).

[16] H. Hu and Q. Si, Coupled topological flat and wide bands: Quasiparticle formation and destruction, Sci. Adv. **9**, eadg0028 (2023).

[17] Y. Liu, Z.-Y. Liu, J.-K. Bao, P.-T. Yang, L.-W. Ji, S.-Q. Wu, Q.-X. Shen, J. Luo, J. Yang, J.-Y. Liu, C.-C. Xu, W.-Z. Yang, W.-L. Chai, J.-Y. Lu, C.-C. Liu, B.-S. Wang, H. Jiang, Q. Tao, Z. Ren, X.-F. Xu, C. Cao, Z.-A. Xu, R. Zhou, J.-G. Cheng, and G.-H. Cao, Superconductivity under pressure in a chromium-based kagome metal, Nature (London) **632**, 1032 (2024).

[18] G. Sangiovanni, Superconductor surprises with strongly interacting electrons, Nature (London) **632**, 988 (2024).

[19] J.-X. Yin, B. Lian, and M. Z. Hasan, Topological kagome magnets and superconductors, Nature (London) **612**, 647 (2022).

[20] B. R. Ortiz, L. C. Gomes, J. R. Morey, M. Winiarski, M. Bordelon, J. S. Mangum, I. W. H. Oswald, J. A. Rodriguez-Rivera, J. R. Neilson, S. D. Wilson, E. Ertekin, T. M. McQueen, and E. S. Toberer, New kagome prototype materials: Discovery of Kv_3Sb_5, RbV_3Sb_5, and CsV_3Sb_5, Phys. Rev. Mater. **3**, 094407 (2019).

[21] B. R. Ortiz, S. M. L. Teicher, Y. Hu, J. L. Zuo, P. M. Sarte, E. C. Schueller, A. M. M. Abeykoon, M. J. Krogstad, S. Rosenkranz, R. Osborn, R. Seshadri, L. Balents, J. He, and S. D. Wilson, CsV_3Sb_5: A $\mathbb{Z}_2$ topological kagome metal with a superconducting ground state, Phys. Rev. Lett. **125**, 247002 (2020).

[22] B. R. Ortiz, P. M. Sarte, E. M. Kenney, M. J. Graf, S. M. L. Teicher, R. Seshadri, and S. D. Wilson, Superconductivity in the $\mathbb{Z}_2$ kagome metal Kv_3Sb_5, Phys. Rev. Mater. **5**, 034801 (2021).

[23] S. D. Wilson and B. R. Ortiz, Av_3Sb_5 kagome superconductors, Nat. Rev. Mater. **9**, 420 (2024).

[24] H. Zhao, H. Li, B. R. Ortiz, S. M. L. Teicher, T. Park, M. Ye, Z. Wang, L. Balents, S. D. Wilson, and I. Zeljkovic, Cascade of correlated electron states in the kagome superconductor CsV_3Sb_5, Nature (London) **599**, 216 (2021).

[25] X. Zhou, Y. Li, X. Fan, J. Hao, Y. Dai, Z. Wang, Y. Yao, and H.-H. Wen, Origin of charge density wave in the kagome metal CsV_3Sb_5 as revealed by optical spectroscopy, Phys. Rev. B **104**, L041101 (2021).

[26] Z. Liang, X. Hou, F. Zhang, W. Ma, P. Wu, Z. Zhang, F. Yu, J.-J. Ying, K. Jiang, L. Shan, Z. Wang, and X.-H. Chen, Three-dimensional charge density wave and surface-dependent vortex-core states in a kagome superconductor CsV_3Sb_5, Phys. Rev. X **11**, 031026 (2021).

[27] E. Uykur, B. R. Ortiz, S. D. Wilson, M. Dressel, and A. A. Tsirlin, Optical detection of the density-wave instability in the kagome metal Kv_3Sb_5, npj Quantum Mater. **7**, 16 (2022).

[28] H. Li, T. T. Zhang, T. Yilmaz, Y. Y. Pai, C. E. Marvinney, A. Said, Q. W. Yin, C. S. Gong, Z. J. Tu, E. Vescovo, C. S. Nelson, R. G. Moore, S. Murakami, H. C. Lei, H. N. Lee, B. J. Lawrie, and H. Miao, Observation of unconventional charge density wave without acoustic phonon anomaly in kagome superconductors AV_3Sb_5 (a = Rb, Cs), Phys. Rev. X **11**, 031050 (2021).

[29] Y. Hu, S. M. Teicher, B. R. Ortiz, Y. Luo, S. Peng, L. Huai, J. Ma, N. C. Plumb, S. D. Wilson, J. He, and M. Shi, Topological surface states and flat bands in the kagome superconductor CsV_3Sb_5, Sci. Bull. **67**, 495 (2022).

[30] J. Kanamori, Electron correlation and ferromagnetism of transition metals, Prog. Theor. Phys. **30**, 275 (1963).

[31] A. Georges, L. d. Medici, and J. Mravlje, Strong correlations from hund's coupling, Annu. Rev. Condens. Matter Phys. **4**, 137 (2013).

[32] C. Xu, S. Wu, G.-X. Zhi, G. Cao, J. Dai, C. Cao, X. Wang, and H.-Q. Lin, Altermagnetic ground state in distorted kagome metal $CsCr_3Sb_5$, Nat. Commun. **16**, 3114 (2025).

[33] G. Kresse and J. Furthmüller, Efficient iterative schemes for *ab initio* total-energy calculations using a plane-wave basis set, Phys. Rev. B **54**, 11169 (1996).

[34] G. Kresse and D. Joubert, From ultrasoft pseudopotentials to the projector augmented-wave method, Phys. Rev. B **59**, 1758 (1999).

[35] J. P. Perdew, K. Burke, and M. Ernzerhof, Generalized gradient approximation made simple, Phys. Rev. Lett. **77**, 3865 (1996).

[36] B. Bradlyn, L. Elcoro, J. Cano, M. G. Vergniory, Z. Wang, C. Felser, M. I. Aroyo, and B. A. Bernevig, Topological quantum chemistry, Nature (London) **547**, 298 (2017).

[37] L. Elcoro, B. Bradlyn, Z. Wang, M. G. Vergniory, J. Cano, C. Felser, B. A. Bernevig, D. Orobengoa, G. de la Flor, and M. I. Aroyo, Double crystallographic groups and their representations on the Bilbao Crystallographic Server, J. Appl. Crystallogr. **50**, 1457 (2017).

[38] G. Pizzi, V. Vitale, R. Arita, S. Blügel, F. Freimuth, G. Géranton, M. Gibertini, D. Gresch, C. Johnson, T. Koretsune, J. Ibañez-Azpiroz, H. Lee, J.-M. Lihm, D. Marchand, A. Marrazzo, Y. Mokrousov, J. I. Mustafa, Y. Nohara, Y. Nomura, L. Paulatto, S. Poncé, T. Ponweiser, J. Qiao, F. Thöle, S. S. Tsirkin, M. Wierzbowska, N. Marzari, D. Vanderbilt, I. Souza, A. A. Mostofi, and J. R. Yates, Wannier90 as a community code: new features and applications, J. Phys.: Condens. Matter **32**, 165902 (2020).

[39] See Supplemental Material at http://link.aps.org/supplemental/10.1103/PhysRevResearch.7.L022061 for the detailed discussion about $U(1)$ slave-spin approach and additional numerical results.

[40] D. Soriano, A. N. Rudenko, M. I. Katsnelson, and M. Rösner, Environmental screening and ligand-field effects to magnetism in CrI_3 monolayer, npj Comput. Mater. **7**, 162 (2021).

[41] L. Vaugier, H. Jiang, and S. Biermann, Hubbard u and hund exchange j in transition metal oxides: Screening versus localization trends from constrained random phase approximation, Phys. Rev. B **86**, 165105 (2012).

[42] R. Yu and Q. Si, $U(1)$ slave-spin theory and its application to mott transition in a multiorbital model for iron pnictides, Phys. Rev. B **86**, 085104 (2012).

[43] R. Yu and Q. Si, Mott transition in multiorbital models for iron pnictides, Phys. Rev. B **84**, 235115 (2011).

[44] H. Lin, R. Yu, J.-X. Zhu, and Q. Si, Orbital-selective correlations and renormalized electronic structure in lifeas, Phys. Rev. B **109**, 075170 (2024).

[45] Y. Wang, Heavy fermions in frustrated hund's metal with portions of incipient flat bands, Phys. Rev. B **111**, 035127 (2025).

[46] Y. Guo, Z. Wang, F. Xie, Y. Huang, B. Gao, J. S. Oh, H. Wu, Z. Liu, Z. Ren, Y. Fang, A. Biswas, Y. Zhang, Z. Yue, C. Hu, C. Jozwiak, A. Bostwick, E. Rotenberg, M. Hashimoto, D. Lu, J. Kono, J.-H. Chu, B. I. Yakobson, R. J. Birgeneau, Q. Si, P. Dai, and M. Yi, Ubiquitous flat bands in a Cr-based kagome superconductor, arXiv:2406.05293.

[47] Y. Li, Y. Liu, X. Du, S. Wu, W. Zhao, K. Zhai, Y. Hu, S. Zhang, H. Chen, J. Liu, Y. Yang, C. Peng, M. Hashimoto, D. Lu, Z. Liu, Y. Wang, Y. Chen, G. Cao, and L. Yang, Electron correlation and incipient flat bands in the kagome superconductor $CsCr_3Sb_5$, Nat. Commun. **16**, 3229 (2025).

[48] S. Peng, Y. Han, Y. Li, J. Shen, Y. Miao, Y. Luo, L. Huai, Z. Ou, H. Li, Z. Xiang, Z. Liu, D. Shen, M. Hashimoto, D. Lu, Y. Yao, Z. Qiao, Z. Wang, and J. He, Flat bands and distinct density wave orders in correlated Kagome superconductor $CsCr_3Sb_5$, arXiv:2406.17769.

[49] I. I. Mazin, H. O. Jeschke, K. Foyevtsova, R. Valentí, and D. I. Khomskii, Na_2IrO_3 as a molecular orbital crystal, Phys. Rev. Lett. **109**, 197201 (2012).

[50] K. Foyevtsova, H. O. Jeschke, I. I. Mazin, D. I. Khomskii, and R. Valentí, *Ab initio* analysis of the tight-binding parameters and magnetic interactions in Na_2IrO_3, Phys. Rev. B **88**, 035107 (2013).

[51] L. Yu, C. Wang, Y. Zhang, M. Sander, S. Ni, Z. Lu, S. Ma, Z. Wang, Z. Zhao, H. Chen, K. Jiang, Y. Zhang, H. Yang, F. Zhou, X. Dong, S. L. Johnson, M. J. Graf, J. Hu, H.-J. Gao, and Z. Zhao, Evidence of a hidden flux phase in the topological kagome metal CsV_3Sb_5, arXiv:2107.10714.

[52] Q. Wu, Z. X. Wang, Q. M. Liu, R. S. Li, S. X. Xu, Q. W. Yin, C. S. Gong, Z. J. Tu, H. C. Lei, T. Dong, and N. L. Wang, Simultaneous formation of two-fold rotation symmetry with charge order in the kagome superconductor CsV_3Sb_5 by optical polarization rotation measurement, Phys. Rev. B **106**, 205109 (2022).

[53] C. Setty, H. Hu, L. Chen, and Q. Si, Electron correlations and t-breaking density wave order in a $\mathbb{Z}_2$ kagome metal, arXiv:2105.15204.